



1 **MANUSCRIPT SUBMITTED TO ACP: GMOS-A**

2 **Title**

3 **A SMART NANOFIBROUS MATERIAL FOR ADSORBING AND REAL-TIME DETECTING ELEMENTAL**  
4 **MERCURY IN AIR**

5 **Authors**

6 Antonella Macagnano<sup>2</sup>, Viviana Perri<sup>1</sup>, Emiliano Zampetti<sup>2</sup>, Andrea Bearzotti<sup>2</sup>, Fabrizio De  
7 Cesare<sup>4</sup>, Francesca Sprovieri<sup>3</sup>, Nicola Pirrone<sup>2</sup>

8 <sup>1</sup>University of Calabria, via Pietro Bucci, Arcavacata, Rende 87036 (CS), Italy; <sup>2</sup>Institute of  
9 Atmospheric Pollution Research-CNR, Via Salaria km 29,300 Montelibretti 00016 (RM), Italy;  
10 <sup>3</sup>Institute of Atmospheric Pollution Research-CNR, Division of Rende, c/o UNICAL-Polifunzionale  
11 Arcavacata, Rende 87036 (CS) Italy; <sup>4</sup>DIBAF-University of Tuscia, Via S. Camillo de Lellis,  
12 01100 Viterbo, Italy

13

14 *Correspondence to:* Antonella Macagnano, [a.macagnano@iia.cnr.it](mailto:a.macagnano@iia.cnr.it); [antonella.macagnano@cnr.it](mailto:antonella.macagnano@cnr.it)

15

16 **Abstract**

17 The combination of gold affinity for mercury with nanosized frameworks has allowed to design  
18 and fabricate novel kinds of sensors with promising sensing features for environmental  
19 applications. Specifically, conductive sensors based on composite nanofibrous electrospun layers  
20 of titania easily decorated with gold nanoparticles were developed to obtain nanostructured  
21 hybrid materials, capable of entrapping and revealing GEM traces from environment. The  
22 electrical properties of the resulting chemosensors were measured. Few minutes of air sampling  
23 were sufficient to detect the concentration of mercury in the air, in the range between 20-100  
24 ppb, without using traps or gas carriers (LOD ~ 1.5 ppb). Longer measurements allowed the sensor  
25 to detect lower concentrations of GEM. The resulting chemosensors are expected to be low-cost,  
26 very stable (due to the peculiar structure), and requiring low power, low maintenance and simple  
27 equipment to work.

28

29 **1 Introduction**

30 Mercury (Hg) is released into the atmosphere both by human's activities, predominantly fossil fuel  
31 combustion, and naturally, for example, from soil out-gassing, volcanoes and evasion from the sea  
32 (Pirrone et al., 2010; Pacyna et al., 2010). One of the more troublesome questions in recent years



33 has been to quantify not only the strength of emission sources but also the effects of re-emission of  
34 previously deposited Hg on the overall distribution, concentration and speciation of Hg in the  
35 atmosphere (Hedgecock et al., 2003). The deposition of atmospheric Hg depends on its chemical  
36 speciation, where the term speciation is used to distinguish between the gaseous elemental (GEM)  
37 and gaseous oxidized forms of Hg [GOM and Particle bound mercury (PBM)] and their chemical-  
38 physical characteristics (Lyman et al., 2010; Sprovieri et al., 2016a,b). To be precise, Total gaseous  
39 mercury (TGM) mainly comprises GEM with minor fractions of other volatile species (e.g., HgO,  
40 HgCl<sub>2</sub>, HgBr<sub>2</sub>, CH<sub>3</sub>HgCl, or (CH<sub>3</sub>)<sub>2</sub>Hg). However, in spite of conceptual differences between TGM  
41 and GEM, they have often been used without clear distinction. This was allowable to a degree as  
42 the predominant fraction of TGM (usually in excess of 99%) is often represented by GEM under  
43 normal conditions. GEM is relatively inert under atmospheric conditions, only slightly soluble and  
44 also quite volatile, whereas the oxidized Hg forms found in the atmosphere are both soluble and  
45 involatile, thus they are efficiently scavenged and consequently deposited by liquid atmospheric  
46 water, such as rain and fog droplets, but also deliquesced aerosol particles. The dispersion of GEM  
47 on global scale therefore, depends on the rate of its oxidation in the atmosphere as this determines  
48 its long atmospheric lifetime (generally >1 year), limiting local emission controls from protecting  
49 all environments. Several international initiatives and programs [i.e., the United Nations  
50 Environment Program (UNEP)] have also made a tremendous effort in identifying and quantifying  
51 Hg pollution across the globe, especially the “hot-spots”, aimed at reducing risk of exposure to this  
52 neurotoxin pollutant. Policy makers are working toward a worldwide effort for supporting the  
53 constructing an accurate global Hg budget and to model the benefits or consequences of changes in  
54 Hg emissions, for example, as proscribed by the Minamata Convention. Anticipating a global  
55 policy, in 2010 the European Commission began a five-year project called the Global Mercury  
56 Observation System (GMOS, [www.gmos.eu](http://www.gmos.eu)) to create a coordinated global network to gaps in  
57 emissions monitoring and in the spatial coverage of environmental observations, mostly in the  
58 tropical regions and Southern Hemisphere, thus adequate for improving models and making policy  
59 recommendations (Sprovieri et al., 2016a,b). To date the GMOS network consists of more 43  
60 monitoring stations worldwide distributed including high altitude and sea level monitoring sites,  
61 and located in climatically diverse regions, including polar areas (Sprovieri et al., 2016a,b). One of  
62 the major outcomes of GMOS has been an interoperable e-infrastructure developed following the  
63 Group on Earth Observations (GEO) data sharing and interoperability principles which allows us to  
64 provide support to UNEP for the implementation of the Minamata Convention (i.e., Article 22).  
65 GMOS activities are currently part of the GEO strategic plan (2016–2025) within the flagship on  
66 “tracking persistent pollutants”. The overall goal of this flagship is to support the development of



67 GEOSS by fostering research and technological development on new advanced sensors for in situ  
68 and satellite platforms, in order to lower the management costs of long-term monitoring programs  
69 and improve spatial coverage of observations. Since automated measurement methods of Hg require  
70 power, argon gas, and significant operator training, they are difficult to apply for understanding Hg  
71 air concentrations and deposition across broad regional and global scales. Therefore, the lack of an  
72 inexpensive, stand-alone, low power, low-maintenance sensor is a primary technical issue to be  
73 solve for the sustainability of a global network such as GMOS. Previous research highlighted that  
74 Hg-concentration levels in air vary greatly across different environmental locations, remote as the  
75 Polar Regions, background or rural, and urban locations with an average range between  $1.5 \text{ ngm}^{-3}$   
76 (GEM) and  $1 \text{ pgm}^{-3}$  (GOM and PBM), depending on the speciation. Hence, for the determination of  
77 atmospheric Hg also at such low levels, sampling and analytical methods should be sensitive  
78 enough to quantify the concentration profiles of diverse Hg species in each respective  
79 environmental setting to better understand their environmental behavior and patterns. Fortunately,  
80 many advances made in analytical methodologies have made it possible to study atmospheric Hg in  
81 different environmental locations. However, several limitations and difficulties have still  
82 experienced in Hg analysis, as most methods cannot yet directly or accurately determine minor Hg  
83 species (Gustin et al., 2013). Hence, efforts should be continued to secure further the reliability, the  
84 traceability, and the accuracy of Hg levels measured in air. Current air monitors are amply sensitive  
85 to detect the global background but are costly, complicated configuration, electricity requirements  
86 and high maintenance. This limits the scientific research community's ability to long-term measure  
87 atmospheric Hg concentrations worldwide. Sampling and analysis of atmospheric Hg is made most  
88 commonly as GEM/TGM because of their greater abundance, even if both manual and automatic  
89 methods have been currently developed for different Hg forms to suit the measurement and  
90 monitoring application. The most common sampling method employed relies on adsorption on gold  
91 amalgam and then, either directly or indirectly, through a stepwise process of thermal desorption  
92 and final detection [usually by cold-fiber atomic absorption spectroscopy (CVAAS) or cold-fiber  
93 atomic fluorescence spectroscopy (CVAFS)]. However, our knowledge presents currently several  
94 gaps to be solved. Firstly, The atmospheric chemistry of Hg remains poorly understood, especially  
95 the oxidation pathways by which GEM is converted to GOM, the reduction pathway which converts  
96 GOM back to GEM, and the gas-particle partitioning. This is partially due to the need for  
97 identification of the chemical forms of oxidized Hg in the atmosphere and methods to measure  
98 these compounds individually. In addition, the limitations and potential interferences with our  
99 current measurement methods have not been adequately investigated, thus alternate methods to  
100 measure atmospheric Hg are needed. Given the uncertainty and restrictions associated with



101 automated and/or semi-automated Hg measurements (Gustin et al., 2013; Pirrone et al., 2013), and  
102 above all, responding to the technical needs of an expanding Hg global observation network, we  
103 developed a reliable, sensitive, and inexpensive surface for atmospheric Hg detection. In particular,  
104 we investigated and demonstrated the utility of composite nanofibrous electrospun layers of titania  
105 decorated with gold nanoparticles (AuNPs) to obtain nanostructured materials capable of adsorbing  
106 GEM as a useful alternative system for making regional and global estimates of air Hg  
107 concentrations. Methods and new sampling systems previously developed, such as passive  
108 samplers, have been used to understand long-term global distribution of persistent organic  
109 pollutants (POPs) (Harner et al., 2003; Pozo et al., 2004). Other passive samplers for both TGM and  
110 GOM collection on the basis of diffusion have been constructed using a variety of synthetic  
111 materials (i.e., gold and silver surfaces, and sulfate-impregnated carbon) and housings (Lyman et  
112 al., 2010; Gustin et al., 2011; Zhang et al., 2012; Huang et al., 2014). However, because of the  
113 differences in design of passive samplers, ambient air Hg concentrations quantified by various  
114 samplers may not be comparable. In addition, sampling rates (SRs) using the same passive samplers  
115 may depend on environmental conditions and atmospheric chemistry at each site. Moreover, it has  
116 been also highlighted that the performance of passive samplers may be influenced by  
117 meteorological factors (e.g., T °C, RH, wind speed) therefore inducing bias for the result of passive  
118 sampling (Plaisance et al., 2004; Sderstrm et al., 2004). On the other hand, incentive for developing  
119 simple and cost-effective samplers that are capable of monitoring over an extended period and  
120 require no technical expertise for deployment of these systems also at remote locations is now  
121 obvious. In this work we describe an alternative approach adopted in the place of conventional ones  
122 demonstrating that the combination of gold affinity for Hg with a nanoscale sized framework of  
123 titania provided the chance to create promising sensors for environmental monitoring in real time,  
124 characterised by high sensitivity to the analyte. The novel sensor is a relatively simple and low cost  
125 method for measurement of the most abundant Hg form in ambient air (TGM/GEM) due to reusable  
126 parts and simple deployment steps. Further, we have evaluated the applicability of this  
127 measurement technique with respect to real environmental conditions highlighting future directions  
128 of research on airborne Hg determination. The TGM/GEM sensor surface described here could be  
129 deployed in a global network such as GMOS; a permanent network of ground based monitoring  
130 sites and observations of Hg and/or related species on a global scale and with remote sensors would  
131 in fact be highly desirable. These data are needed to test and validate model processes and  
132 predictions, understand the source-receptor relationships, understand long-term changes in the  
133 global Hg cycle, and at least, would help policy makers to set regulations for different areas. The  
134 sensor features are related to the nanofibrous scaffold of titania capable of growing up gold



135 nanostructures by photocatalysis, tunable in size and shape. Such a nanostructured layer, fabricated  
136 by electrospinning technology, firstly improves sensor features with respect to those of compact  
137 films, by enhancing the global number of binding sites of analyte-sensor and reducing some bulk  
138 drawbacks. Secondly, the combination of metal oxides and metal nanostructures, improves the  
139 sensitivity, allows sensor to work at room temperature, tunes selectivity towards different gas  
140 species by adjusting the surface to volume ratio of nanosized structures and affect sensor lifetime.  
141 Morphological, optical, electrical aspects and sensing measurements of fibers of GEM in air have  
142 been reported and discussed. When designed, the resulting Hg ad-absorbent material was expected  
143 to be suitable for novel Hg sensors fabrication, since a similar nanofibrous scaffold doped with  
144 AuNPs was described in literature as filtering systems capable of adsorbing and removal Hg fiber  
145 from the environment with an efficiency of about 100% (Y Yuan et al., 2012). In fact, in previous  
146 works (Macagnano et al., submitted, Macagnano et al., 2015a) the authors reported the ultra-high  
147 sensitivity of the sensor, capable to detect up to dozens ppt, despite of a long time necessary to  
148 reveal the analyte at these concentrations, in air. In this work the chance to apply the sensor in  
149 polluted sites and in real time has been presented and described.

150

## 151 **2 Materials and methods**

### 152 *2.1. Chemicals*

153 All chemicals were purchased from Sigma-Aldrich and used without further purification:  
154 polyvinylpyrrolidone (PVP, Mn 1,300,000), titanium isopropoxide (TiiP, 99.999%), gold(III)  
155 chloride hydrate ( $\text{HAuCl}_4$ , 99.999%), anhydrous ethanol ( $\text{EtOH}_a$ ) and glacial acetic acid ( $\text{AcAc}_g$ ).  
156 Ultrapure water ( $5.5 \cdot 10^{-8} \text{ S cm}^{-1}$ ) was produced by MilliQ-EMD Millipore.

### 157 *2.2. Electrospinning technology*

158 Electrospinning is a widely used technique for the electrostatic production of nanofibers, during  
159 which an electric field is used to make polymer fibers with diameters ranging from 2 nm to some  
160 micrometres from polymer solutions (or melts). It is currently the most economic, versatile, and  
161 efficient technology to fabricate highly porous membranes made of nano and/or micro fibers also  
162 for sensors (Macagnano et al., 2015b). It is based on the application of a high voltage difference  
163 between a spinneret ejecting a polymeric solution and a grounded collector. The jet of solution is  
164 accelerated and stretched by the external electric field while travelling towards the collector, leading  
165 to the creation of continuous solid fibers as the solvent evaporates. The electrospinning apparatus  
166 used in the present study (designed and assembled in CNR laboratories) comprised a home-made  
167 clean box equipped with temperature and humidity sensors, a syringe pump (KDS 200, KD  
168 Scientific) and a grounded rotating cylindrical collector (45 mm diameter), a high voltage oscillator



169 (100 V) driving a high voltage (ranging from 1 to 50 kV) and a high power AC-DC (alternative  
170 current-direct current) converter. Electrospinning solution ( $7.877 \times 10^{-5}$  M), was prepared by  
171 dissolving PVP in EtOH<sub>a</sub> and stirring (2 hours). A 2 ml aliquot of 1:4 (w/v) solution of TiiP solved  
172 in 1:1 (v/v) mixture of AcAc<sub>g</sub> and EtOH<sub>a</sub> was freshly prepared and added to 2.5 ml PVP solution  
173 under stirring in order to obtain a 1.95 (w/w) TiiP/PVP final ratio. Both mixtures were prepared in a  
174 glove box under low humidity rate (<7% RH). The syringe filled with the TiiP/PVP solution and  
175 housed in the syringe pump, was connected to a positive DC-voltage (6 kV), and set to a 15 cm far  
176 grounded rotating collector. The substrates were fixed through suitable holders onto the collector  
177 (600 rpm, 21 °C and 35% RH) and processed (feed rate 150 ml h<sup>-1</sup>) for 20 min to obtain scaffolds  
178 for sensors. After deposition, PVP/TiO<sub>2</sub> composite nanofibers were left for some hours at room  
179 temperature to undergo fully self-hydrolysis of TiiP [Li et al., 2003]. And then annealed under  
180 oxygen atmosphere (muffle furnace) using a thermal ramp from room temperature up to 550 °C (1  
181 °C min<sup>-1</sup>, 4 h dwell time) in order to remove PVP and crystallize the metal oxide (*anatase*).

### 182 2.3 Transducers: interdigitated electrodes

183 The transducer adopted in the present work to convert the physico-chemical interactions of analytes  
184 with the different polymer fibers in an electrical signal was an interdigitated electrode (IDE) [Bakir  
185 et al,1973; James et al., 2013]. Specifically, the transducer consisted of 40 pairs of electrodes (150  
186 nm in electrode thickness, 20 μm in gap and electrode width and 5620 μm in length) was  
187 manufactured in CNR laboratories through a standard photolithographic process (lift-off  
188 procedure), then followed by Ti sputtering and Pt e-fiberation, suitable to generate the electrodes of  
189 the size reported above, on a 4 in. oxidised silicon wafer. After electrospinning deposition all the  
190 electrical signals of the resulting chemoresistors were recorded by an electrometer (Keithley 6517  
191 Electrometer).

### 192 2.4 Titania nanofibers

193 Upon calcination, the diameters of fibers extraordinarily shrunk: mean diameters of fibers were  
194 estimated through image analyses to be approximately within the range of 60–80 nm. Specifically,  
195 the resulting fibers appeared fine and rough at surface, with a fairly homogeneous fabric. The  
196 absence of beads and the good quality of the long and continuous fibers was confirmed through  
197 SEM micrographs. A highly porous and dense network of nanofibers covering the electrodes was  
198 observed, showing interconnected void volumes (porosity) and high surface-to-volume ratios  
199 (specific surface area). Zampetti et al., (2013) reported that such a fibrous layer showed a 99% of  
200 pores having an area less than 10 μm<sup>2</sup>, with more than 80% pores being <1 μm<sup>2</sup>.

### 201 2.5 AuNPs/TiO<sub>2</sub>NFs photocatalytic decoration



202 Exploiting the photocatalytic properties of TiO<sub>2</sub>, gold nanoparticles were selectively grown, under  
203 UV-light irradiation, on the electrospun titania nanofibers through the photoreduction of HAuCl<sub>4</sub> in  
204 the presence of an organic capping reagent (PVP). Thus the resulting fibrous scaffolds were dipped  
205 into an aqueous solution containing HAuCl<sub>4</sub> and PVP (1.5·10<sup>-3</sup>M and 0.1M respectively) and  
206 exposed to UV light irradiation for specified intervals (UV lamp (365 nm) (Helios, Italquartz)).  
207 Depending on the gold nanoparticles size that were forming in photocatalysis, the dip-solution  
208 changed from light yellow to purple. Samples were rinsed extensively with water and then air-dried.  
209 Before morphological, electrical and sensing measurements, samples were heated at 450 °C per 1 h  
210 to eliminate the PVP traces. Morphological characterization were provided by scanning electron  
211 microscopy (SEM) (Jeol, JSM 5200, 20 keV) with pictures captured at 5 kV accelerating voltage.  
212 AFM (atomic force microscopy) micrographs were taken in tapping mode using 190Al-G tips, 190  
213 kHz, 48N/m (Nanosurf FlexAFM). TEM (C-TEM, control transmission electron microscopy)  
214 micrographs were performed at 200 keV with an analytical double tilt probe. TEM specimen were  
215 prepared by gently scraping at first the TiO<sub>2</sub> nanofibrous layer electrospun onto the silicon support  
216 and then collecting the nanofibers, through adhesion upon contact with holy carbon thin film. UV-  
217 Vis spectra were provided by Spectrophotometer UV-2600 (Shimadzu), analysing quartz slices  
218 coated with nanofibers. These substrates were able to collect fibers by electrospinning (20 min), and  
219 then were subjected to calcination according to the described above procedure, and then UV  
220 irradiation in the aqueous solution. The fibrous layer stayed stuck to the substrate if the thickness  
221 was thin enough. Longer depositions caused curling of fibers during the calcination process.

### 222 2.5 Measurement set-up

223 The sensor was placed in a suitable PTFE-made measurement chamber (0.7 ml volume) connected  
224 to an electrometer (Keithley 6517 Electrometer) capable of measuring the current flowing through  
225 the IDE, when a fixed potential was applied to it, and to send data to a PC. Dynamic measurements  
226 were carried out at room temperature both using: (i) 4 channel MKS 247 managing four MKS mass  
227 flow controllers (MFC), set in the range 0–200 sccm and (ii) Environics S4000 (Environics, Inc.)  
228 flow controller, containing three MFCs supplying different flow rates (up to 500, 250 and 25 sccm,  
229 respectively), managed by its own software. Pure air (5.0) (Praxair–Rivoira, Italy) was used as gas  
230 carrier. A homemade PTFE (polytetrafluoroethylene) permeation tube filled with a suitable amount  
231 of Hg<sup>0</sup> was included within such a delivery system to get set dilutions of Hg-saturated vapours. The  
232 tube was immersed in a thermostatically controlled bath, thus the desired Hg<sup>0</sup> concentration  
233 delivered to the sensor was achieved by both tuning the temperature of the permeation tube and the  
234 dilution flow. The Hg<sup>0</sup> concentration was checked by Tekran®2537A analyser. Responses were  
235 calculated as  $\Delta I/I_0$ , where  $\Delta I$  was the current variation and  $I_0$  was the current when synthetic pure





236 dry air was flowed. Sensor was restored after a quick thermal shot at 450°C under flow of pure air  
237 (450°C).

238

### 239 3 Results and Discussion

240 Nonwoven mats made of PVP and amorphous TiO<sub>2</sub> were obtained by the combination of  
241 electrospinning and sol-gel techniques (Fig. 1). The deposition occurred for 20 min on oxidised  
242 silicon wafers and IDEs, properly fixed on the surface of a conducting rotating collector to form  
243 nanofibrous layers characterized by high surface areas and relatively small pore sizes (Zampetti et  
244 al.,2013). By changing the deposition time, both thickness and consistence of the mats changed: one  
245 hour deposition provided the formation of a thicker white and soft fabric easily peeled off (Fig.1),  
246 hygroscopic and soluble in both water and polar solvents; a 20 min deposition generated a fibrous  
247 film adhering to substrates, too thin to be weeded. The calcination process caused a complete  
248 degradation of PVP with formation of crystalline TiO<sub>2</sub> (*anatase*) and a significant shrinkage of  
249 fibers dimension (60-80 nm diameter, 5-40 nm grain size). Exploiting the photocatalytic properties  
250 of titania (*anatase*), a tunable decoration of fibers with gold nanoparticle could be achieved by  
251 dipping the fibrous mats in a proper aqueous solution (HAuCl<sub>4</sub>, PVP) under UV light irradiation (Li  
252 et al, 2004; Macagnano et al., 2015). The photocatalytic reaction was proved by the color of the  
253 solution (red purple from light yellow) (Fig.1). Changing both UV irradiation exposure time and  
254 PVP concentration, as capping reagent, morphology, size and density of gold nanoparticles could be  
255 tuned [Macagnano et al., submitted].

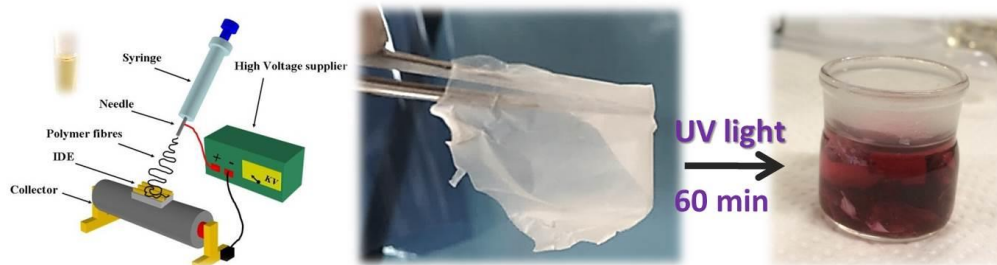


Figure 1. Sketch of an electrospinning set-up comprising a syringe and a grounded rotating cylinder collector where the samples take place for their coverage (*left*); a piece of a nanofibrous fabric of Ti<sub>ii</sub>P/PVP peeled from the substrate after 1 hour of electrospinning deposition (*centre*) a red-purple aqueous solution of HAuCl<sub>4</sub>/PVP after UV-light irradiation treatment holding a piece of the nanofibrous fabric of TiO<sub>2</sub> (*anatase*) obtained after Ti<sub>ii</sub>P/PVP annealing (*right*)

256

257 In the present work, among a series of differently coated fibrous layers, only the fibrous  
258 nanocomposites that were conductive at room temperature were selected and then their electrical  
259 and sensing features investigated. The controlled gold deposition was due to the photo-excited  
260 electrons on the surface of TiO<sub>2</sub> nanofibers that were able to reduce the gold ions thus inducing gold  
261 deposition (Fig. 2, *the sketch*). The capping reagent was responsible of the shape of the particles.





262 The surfaces of nanofibers observed in SEM micrographs (Fig.2, *right*) appeared densely decorated  
263 with globular nanoparticles. In C-TEM image (Fig.2, *inset*) the gold nanoparticles appeared darker  
264 and spherical or quasi-spherical. The single particles size were ranging between 2 and 20 nm, with a  
265  $7.8 \pm 3$  nm average diameter [Macagnano et al., submitted]. Gold nanoparticles grew directly onto  
266 the nanofibers and their adhesion appeared relatively strong (despite due to van der Waals forces),  
267 since they both resisted to water rinsing and fibers scratching for TEM analyses.  
268

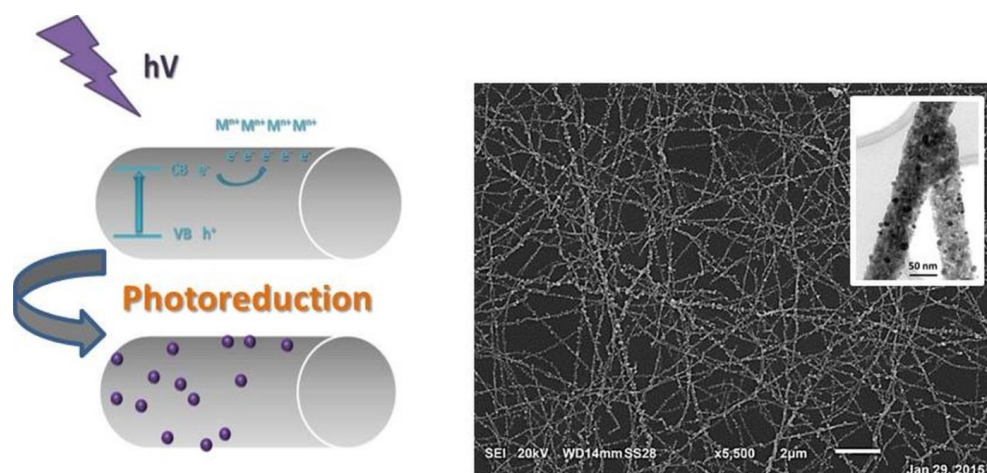


Figure 2. A sketch of the photocatalytic process occurring on the fibers surface (*left*); SEM picture of a dense nanofibrous network of AuNPs/TiO<sub>2</sub> coating a silicon wafer (*right*); a C-TEM micrograph of fibers finely decorated with gold nanoparticles (*the darkest ones*) fixed without using any additional linker (*inset*).

269  
270 After photocatalytic process, the white porous mat became purple-violet. As seen in the spectrum of  
271 the AuNP/TiO<sub>2</sub> system, a characteristic absorbance band appeared at around 543 nm, which  
272 corresponded to the surface plasmon resonance (SPR) of the AuNPs (Sun et al, 2003). A red  
273 shifting and broadening of the absorbance band was observed with the increasing in AuNP size and  
274 fiber loading, respectively (data not shown). The colour is strictly depending on the size of the  
275 nanoparticles, and then their agglomeration at the solid state. According to Bui et al. (2007), such a  
276 band broadening phenomenon is due to the electric dipole–dipole interactions and coupling  
277 occurring between the plasmons of neighbouring particles, whereas nanoparticle agglomeration  
278 phenomena occurred.  
279

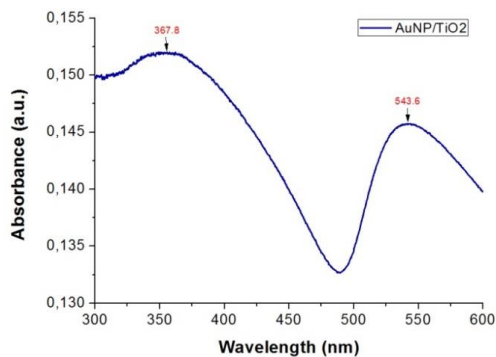


Figure 3. UV-Vis spectrum of a titania nanofibrous network after gold decoration (TiO<sub>2</sub>: 367.8 nm; Au NPs: 543.6 nm)

280

281 Due to these features, UV-Vis absorption spectroscopy has been used in literature as a technique to  
282 reveal the changes in size, shape and aggregation of metal nanoparticles in liquid suspension after  
283 exposure to heavy metals, as Hg<sup>0</sup> (Morris et al., 2002). Both blue-shifted wavelength and its extent  
284 were proportional to the amount of Hg<sup>0</sup> that entered the liquid suspension. Similarly, when the gold  
285 decorated nanofibers of titania, collected on a quartz slice, were exposed to Hg<sup>0</sup> vapours (2 ppm) in  
286 air for 15 min, a significant blue shifting was reported (~ 3 nm) (Fig. 4) due to the atomic  
287 adsorption of GEM on the surface. The nanoparticles could be regenerated by heating the sample at  
288 550°C for 3 minutes to remove Hg<sup>0</sup>. The recovery of the AuNPs was stated by the achieving of the  
289 original values of wavelength. The regeneration could be done for dozen times without any  
290 deterioration. Similarly, in chemoresistors, the TiO<sub>2</sub> nanofibrous layers attached to the substrates  
291 (Fig. 5), changed colour after photocatalytic treatment.

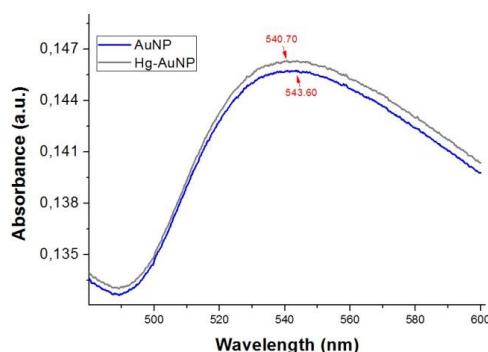


Figure 4. UV-Vis spectra of AuNPs/TiO<sub>2</sub> nanofibers before (blue) and after a 15 min exposure to 2 ppm of Hg<sup>0</sup> (gray)

292



293 The IDE layout (Fig.5) show a set of interdigitated electrodes which occupies an area  
294 approximately 3x5 mm, completely coated with the sensitive fibers, and two bonding pads (2x2  
295 mm) that will be connected to the electrometer (DC voltage). Such a planar interdigitated electrode  
296 configuration is the most commonly used for conductometric sensing applications.

297

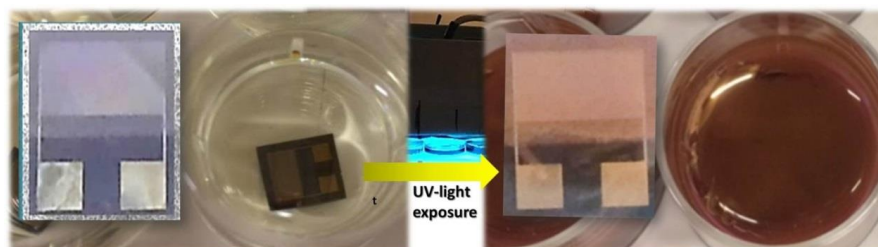


Figure 5. Chemosensor fabrication and final structure: IDE dipped (*left*) and exposed to UV-light (*right*) for gold decoration

298

299 Figure 6 depicts a Current–Voltage (I–V) curve of a chemosensor, under synthetic dry air. However  
300 curve shape was unaltered when air or nitrogen were flushed over the fibers (Macagnano et al.,  
301 2015), suggesting that oxygen concentrations poorly affected the electrical properties of such a  
302 chemoresistor. The resistance value of IDE coated with TiO<sub>2</sub> nanofibers before photocatalysis,  
303 resulted to be too high at room temperature to contribute straight to the final current. The resulting  
304 linear shape (Ohmic behaviour) within the selected voltage range (–3V to +3V) showed a constant  
305 resistance value for the sensor. The very low value of resistance (~1.2 kΩ) provided the chance to  
306 work at low voltage, with consequent effects on the energy consumption as well as lifetime of the  
307 material. Moreover, the linearity of I–V curve let us suppose that the sensing scaffold had a good  
308 adhesion to the metal electrodes. The electron conductivity has been described by the percolation  
309 model (Macagnano et al, submitted; Muller et al., 2003) since the titania at room temperature was  
310 supposed like an insulating organic matrix. When it is metal doped, the electron conductivity is  
311 ruled by thermally activated electron tunneling from one metal island (gold nanoparticles) to the  
312 other. However, the conductivity of the nanocomposite is lower than that of pure metal (gold)  
313 because the electron mean free path is greatly reduced due to the presence of the dielectric (the  
314 titania crystals). The electrical features, such as the reproducibility of the fabrication process, of this  
315 conductive device have been previously investigated by the authors (Macagnano et al, submitted;  
316 Macagnano et al., 2015), showing encouraging results for the development of a low cost sensor for  
317 mercury detection. However, in spite of the high sensitivity (LOD: 2ppt) of the sensor, too long  
318 response time was necessary to detect traces of Hg<sup>0</sup>, when compared to the current monitoring  
319 instrumentations (Ghaedi et al., 2006; Sanchez-Rodas et al., 2010; Ferrua et al., 2007). Extremely



320 encouraging resulted if compared to other sensors currently involved in detecting mercury in air  
321 (Drelich et al., 2008; Kabir et al., 2015; Sabri et al., 2009; Mohibul Kabir et al., 2015; Raffa et al.,  
322 2006; James et al., 2012-2013; Chemnasiri et al., 2012; Sabri et al., 2011; Keebaugh et al., 2007;  
323 Crosby, 2013; McNicholas et al., 2011). The long time in response was supposed to be in part due  
324 to the layout of the measuring system, since the sensor was housed in a quartz bottle of 100 mL  
325 volume. In fact, an additional time was expected to be caused by the adsorption of the  $\text{Hg}^0$  traces  
326 from the surrounding environment (measuring chamber) up to achieve a sufficient number of  
327 mercury atoms adsorbed on the surface sensor to be electrically revealed. In the present study the  
328 measuring chamber was designed in order to reduce the volume (0.7 mL) and to expose the fibers to  
329 the gas entry (Fig. 7). Such a measuring layout was designed to allow the fibrous network to be  
330 exposed to the mercury atoms as delivered into the sensor chamber.  
331

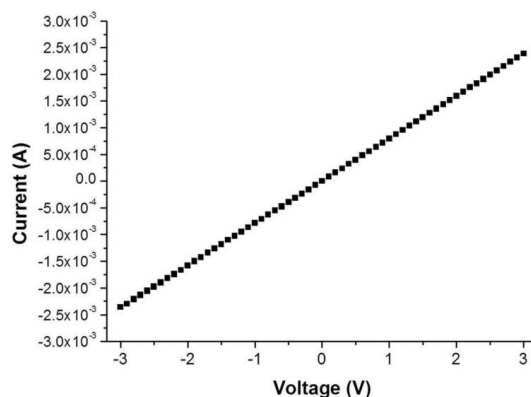


Figure 6. Chemosensor current-voltage curve

332 Sensing measurements, i.e. current (or resistance) changes, were provided in continuous. The  
333 sensor measurements, that were the electrical signals reported when interaction between the sensing  
334 layers and the analytes were happening, resulted in a change of the whole current (or resistance, i.e.  
335  $I = V/R$ ) according to Ohm's law. The sensor was exposed to a flow of  $\text{Hg}^0$  in air with a  
336 concentration of 800 ppb for 1 min (Fig. 7, right), and then air was used to clean the sensor surface.  
337 A rapid decrease in current was recorded ( $1.056 \cdot 10^{-7} \text{ A} \cdot \text{s}^{-1}$ ) when  $\text{Hg}^0$  entered the measuring  
338 chamber. The current curve trend slightly changed when clean air was flowed, stabilizing at about  
339 the current values reached for  $\text{Hg}^0$  adsorption. Due to the strong affinity between Au and  $\text{Hg}^0$ , a 3  
340 min-thermal treatment was necessary to remove mercury from layer and get the same starting  
341 current value.  
342  
343

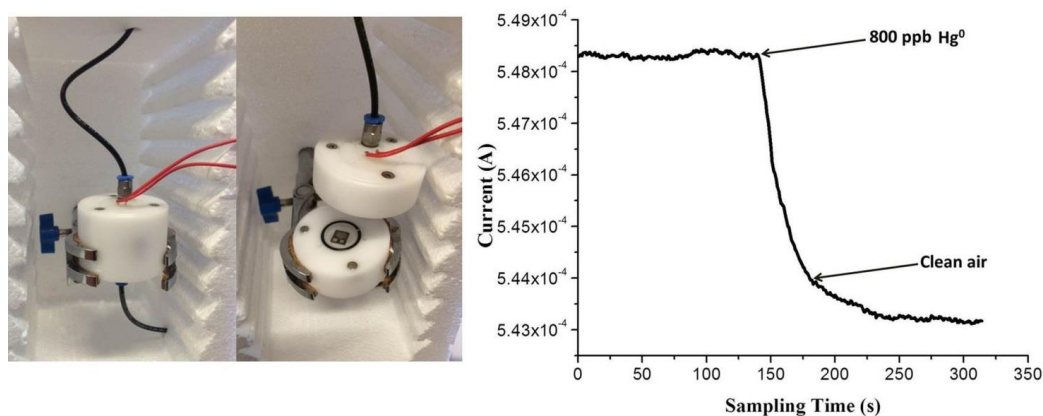


Figure 7. Homemade measurement chamber to house the chemosensor for laboratory experiments (left); plot depicting the transient response curve to 800 ppb  $\text{Hg}^0$  ( $V=0.3$  V)

344

345

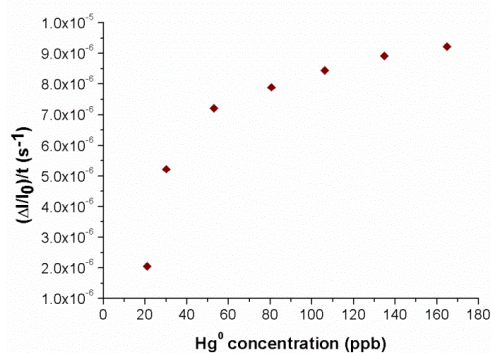


Figure 8. The normalized sensor response rate to the increasing concentration of vapour elemental mercury

346

347 Figure 8 depicts the normalized sensor response rate, i.e. the normalized current change per second,  
348 toward the increasing concentration of GEM (ranging between 20 and 160 ppb). The resulting  
349 logarithmic curve describes how the  $\text{Hg}^0$  concentration affects the response time: small variations of  
350  $\text{Hg}^0$  concentration up to 80 ppb are able to deeply change the response rate, on the contrary higher  
351 concentration seem to affect only slightly this sensing feature. Since a strong relationship is  
352 recorded between the concentration and the response time when the content of mercury in  
353 environment is low, is possible to correlate the slope of the transient responses within the first  
354 minutes of the sensor response to definite concentrations of  $\text{Hg}^0$  in air. Figure 9 depicts the linear  
355 fitting of 10 min-sensor responses when increasing concentrations of mercury were flowed onto the  
356 sensor. Related data were reported in Table 1.

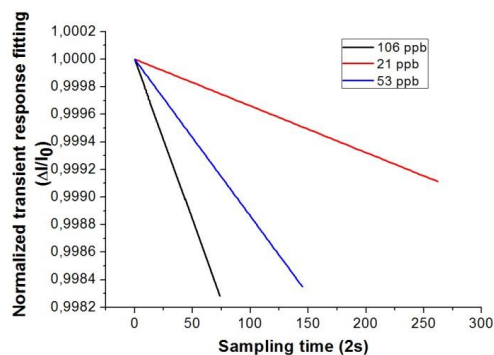


Figure 9. Linear fitting of the normalized sensor response within the first ten minutes

357

358

359

**Table 1. Linear fitting parameters of 10 min-sensor responses to 21 ppb ≤ [Hg<sup>0</sup>] ≤ 106 ppb**

ppb	( $\Delta I/I_0$ )s <sup>-1</sup>	SE(±)	R <sup>2</sup>
21	-7.12602E-10	1.75521E-11	0.86
33	-1.50647E-9	1.05521E-10	0.91
39	-1.78067E-9	1.02615E-10	0.91
40	-1.85901E-9	1.01833E-10	0.92
53	-2.44657E-9	4.24993E-11	0.91
70	-3.19082E-9	2.55882E-11	0.93
106	-4.83599E-9	2.67462E-10	0.88

360

361 A linear relationships has been reported between the response rate and the concentration of Hg,

362 according to the following equation (1):

363 (1)  $y = (-4.56226E^{-11}) \cdot [Hg^0]$ ,  $[Hg^0] < 100 \text{ ppb}$ ;  $SE: \pm 1.504E^{-12}$ ;  $R^2 = 0.99675$

364



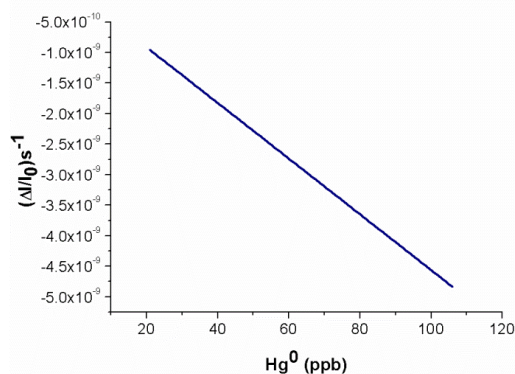


Figure 10. Linear relationships between the normalized response time and the Hg<sup>0</sup> concentration, within the range of 20 and 100 ppb.

365

366 Therefore when the concentration of Hg increased, the response curve slope changed too linearly,  
367 allowing a limit of detection of about 1 ppb, when the sensor is exposed to air polluted with Hg<sup>0</sup> per  
368 10 min. For what concerns main interfering compounds, since at room temperature and in dark  
369 condition the measured current is supposed to be due to AuNPs decorating titania fibers, only  
370 chemical compounds interacting with gold are expected to be mostly responsible of the current  
371 changes (i.e. halides and sulphides). Thus in a blend of other chemicals, this sensor has been  
372 designed as a pretty selective sensor, being able to greatly decrease the environmental disturbances  
373 allowing the investigator/manufacturer to design and then fabricate easier strategies to prevent  
374 contaminations from environment (selective filtering systems or coatings). Among common  
375 potential contaminants authors investigated previously water vapour influence (%RH) reporting no-  
376 effects on the electrical signals (Macagnano et al., 2015).

377

#### 378 4 Conclusions

379 The adopted sensing strategy has focused on the strong affinity of mercury to gold combined to  
380 the nanostructures properties. Exploiting the photocatalytic properties of electrospun titania  
381 nanofibers, a novel conductometric sensor has been designed and fabricated to detect GEM in air.  
382 Electrospinning technology has been used successfully to create a 3D-framework of titania  
383 covering the electrode sensing area of the properly designed chemoresistors (IDEs). AuNPs have  
384 been grown on TiO<sub>2</sub> nanofibers exploiting the photocatalytic properties. Such a sensor was able to  
385 work at room temperature and was highly sensitive to Hg<sup>0</sup>. Since it is composed of titania and  
386 gold, it sounds to be robust and resistant to common solvents and VOCs commonly in the air. The



387 short thermal treatments (450°C, 3min), necessary to desorb mercury from AuNPs, didn't seem to  
388 affect the lifetime of the device. Depending on the strategy of sampling, a sensing device based on  
389 such a chemosensor, could be designed for real applications, specifically for real time monitoring  
390 of polluted sites. Few minutes of sampling of air are sufficient to quantify the concentration of  
391 mercury in the air, in the range between 20-100 ppb (LOD: 1 ppb), without using traps or gas  
392 carriers. However further investigations are necessary also to assess the effects of physical  
393 parameters of the environment, such as temperature fluctuations and UV-light, as well as  
394 chemical ones, such as volatile organic compounds and gas (like halides and sulphides) which are  
395 well known interfering of the adsorption process of the Hg<sup>0</sup> on gold.

396

#### 397 **Acknowledgments**

398 The activity is part of the International UNEP-Mercury Programme (UNEP-Mercury Air Transport  
399 and Fate Research (UNEP-MFTP) within the framework Global Mercury Observation System,  
400 funded by EC as part of EC FP7. Furthermore, authors gratefully thank Mr. Giulio Esposito and Mr.  
401 A. Capocecera for their support in the use of laboratory instrumentations.

402

#### 403 **References**

404 Bui, M.P., Baek, T.J., Seong, G.H., 2007. Gold nanoparticle aggregation-based highly sensitive  
405 DNA detection using atomic force microscopy. *Anal. Bioanal. Chem.* 388, 1185–1190

406 Chemnasiri, W., Hernandez, FE., 2012. Gold nanorod-based mercury sensor using functionalized  
407 glass substrates, *Sensors and Actuators B* 173, 322–328

408 Crosby, J., 2013. Mercury Detection with Gold Nanoparticles. Electronic Thesis and Dissertations  
409 UC Berkeley <http://eprints.cdlib.org/uc/item/3s40h5m0>

410 Drelich, J., White, C. L., Xu, Z., 2008. Laboratory Tests on Mercury Emission Monitoring with  
411 Resonating Gold-coated Silicon Cantilevers. *Environ. Sci. Technol.* 42 2072–2078

412 Ferrua, N., Cerutti, S., Salonia, J. A., Olsina, R. A. and Martinez, L. D., 2007. On-line  
413 preconcentration and determination of mercury in biological and environmental samples by cold  
414 fiber-atomic absorption spectrometry. *J. Hazard. Mater.* 141 693–699

415 Ghaedi, M., Fathi, MR., Shokrollahi, A., Shajarat, F., 2006. Highly Selective and Sensitive  
416 Preconcentration of Mercury Ion and Determination by Cold Fiber Atomic Absorption  
417 Spectroscopy. *Analytical Letters* 39, 1171-1185

418 Gustin, M.S., Huang, J., Miller, M.B., Peterson, C., Jaffe, D.A., Ambrose, J., Finley, B.D., Lyman,  
419 S.N., Call, K., Talbot, R., Feddersen, D., Mao, H., Lindberg, S.E., 2013. Do we understand what the  
420 mercury speciation instruments are actually measuring? Results of RAMIX. *Environ. Sci. Technol.*  
421 47, 7295-7306.

422



- 423 Gustin, M.S., Lyman, S.N., Kilner, P., Prestbo, E., 2011. Development of a passive sampler for  
424 gaseous mercury. *Atmos. Environ.* 45, 5805-5812.  
425
- 426 Harner, T., Farrar, N.J., Shoeib, M., Jones, K.C., Gobas, F., 2003. Characterization of polymer-  
427 coated glass as a passive air sampler for persistent organic pollutants. *Environ. Sci. Technol.* 37,  
428 2486-2493.  
429
- 430 Hedgecock, I., Pirrone, N., Sprovieri, F., Pesenti, E. (2003) Reactive Gaseous Mercury in the  
431 Marine Boundary Layer: Modeling and Experimental Evidence of its Formation in the  
432 Mediterranean. *Atmospheric Environment*, 37/S1, 41-49.
- 433 Huang, J., Lyman, S.N., Hartman, J.S., Gustin, M.S., 2014. A review of passive sampling systems  
434 for ambient air mercury measurements. *Environ. Sci. Process. Impacts* 16, 374-392.  
435
- 436 James, J.Z., Lucas, D., Koshland, C.P., 2012. Gold Nanoparticle Films As Sensitive and Reusable  
437 Elemental Mercury Sensors. *Environ. Sci. Technol.* 46 (2012) 9557–9562
- 438 James, J.Z., Lucas, D., Koshland, C.P., 2013. Elemental mercury fiber interaction with individual  
439 gold nanorods, *Analyst* 138, 2323-2328
- 440 Kabir, K., Sabri, Y., Matthews, G., Jones, L., Ippolito, S., Bhargava, S. 2015. Selective detection of  
441 elemental mercury fiber using a surface acoustic wave (SAW) sensor. *Analyst*, 140, 5508-5517
- 442 Keebaugh, S., Nam, W.J., Fonash, S.J., 2007. Manufacturable Highly Responsive Gold Nanowire  
443 Mercury Sensors, *NSTI-Nanotech* 3, 33-36, [www.nsti.org](http://www.nsti.org)
- 444 Li, D., McCann, J.T., Gratt, M., Xia, Y., 2004. Photocatalytic deposition of gold nanoparticles on  
445 electrospun nanofibers of titania, *Chemical Physics Letters* 394, 387–391
- 446 Lyman, S.N., Gustin, M.S., Prestbo, E.M., 2010. A passive sampler for ambient gaseous oxidized  
447 mercury concentrations. *Atmos. Environ.* 44, 246-252.  
448
- 449 Macagnano, A., Zampetti, E., Kny, E., 2015b. *Electrospinning for High Performance Sensors*,  
450 Springer International Publishing, pp. 1-329.
- 451 Macagnano, A., Zampetti, E., Perri, V., Bearzotti, A., Sprovieri, F., Pirrone, N., Esposito, G., De  
452 Cesare, F., 2015a. Photocatalytically Decorated Au-nanoclusters TiO<sub>2</sub> Nanofibers for Elemental  
453 Mercury Fiber Detection, *Procedia Engineering* 120, 422–426
- 454 Macagnano, A., Perri, V., Zampetti, E., Bearzotti, A., Ferretti, A.M., Sprovieri, F., Esposito, G.,  
455 Pirrone, N., De Cesare, F., Elemental mercury vapour chemoresistors employing TiO<sub>2</sub> nanofibers  
456 photocatalytically decorated with Au-Nanoparticles, *submitted to Sensors and Actuators B*.
- 457 McNicholas, T.P., Zhao, K., Yang, C., Hernandez, S.C., Mulchandani, A., Myung, N.V., Deshusses,  
458 M.A., 2011. Sensitive Detection of Elemental Mercury Fiber by Gold-Nanoparticle-Decorated  
459 Carbon Nanotube Sensors, *J. Phys. Chem. C* 115, 13927–13931
- 460 Mohibul Kabir, K.M., Ippolito, S.J., Matthews, G.I., Abd Hamid, S.B., Sabri, Y.M., Bhargava,  
461 S.K., 2015. Determining the Optimum Exposure and Recovery Periods for Efficient Operation of a  
462 QCM Based Elemental Mercury Fiber, *Sensor Journal of Sensors* 727432-9
- 463 Morris, T., Klopper, K., Wilson, S., Szulczewsk, G., 2002. A Spectroscopic Study of Mercury  
464 Fiber Adsorption on Gold Nanoparticle Films, *Journal of Colloid and Interface Science* 254, 49–55



- 465 Pacyna, E., Pacyna, J., Sundseth, K., Munthe, J., Kindbom, K., Wilson, S., Steenhuisen, F., and  
466 Maxson, P.: Global emission of mercury to the atmosphere from anthropogenic sources in 2005 and  
467 projections to 2020, *Atmos. Environ.*, 44, 2487–2499, doi:10.1016/j.atmosenv.2009.06.009, 2010.  
468
- 469 Pirrone, N., Cinnirella, S., Feng, X., Finkelman, R., Friedli, H., Leaner, J., Mason, R., Mukherjee,  
470 A., Stracher, G., Streets, D., and Telmer, K.: Global mercury emissions to the atmosphere from  
471 anthropogenic and natural sources, *Atmos. Chem. Phys.*, 10, 5951–5964, doi:10.5194/acp-10-5951-  
472 2010, 2010  
473
- 474 Pirrone, N., Aas, W., Cinnirella, S., Ebinghaus, R., Hedgecock, I.M., Pacyna, J., Sprovieri, F.,  
475 Sunderland, E.M., 2013. Toward the next generation of air quality monitoring: mercury. *Atmos.*  
476 *Environ.* 80, 599-611.  
477
- 478 Plaisance, H., Piechocki-Minguy, A., Gracia-Fouque, S., Galloo, J.C., 2004. Influence of  
479 meteorological factors on the NO<sub>2</sub> measurements by passive diffusion tube. *Atmos. Environ.* 38,  
480 573-580.  
481
- 482 Pozo, K., Harner, T., Shoeib, M., Urrutia, R., Barra, R., Parra, O., Focardi, S., 2004. Passive-  
483 sampler derived air concentrations of persistent organic pollutants on a north-south transect in  
484 Chile. *Environ. Sci. Technol.* 38, 6529-6537.  
485
- 486 Raffa, V., Mazzolai, B., Mattoli, V., Mondini, A., Dario, P., 2006. Model validation of a mercury  
487 sensor, based on the resistivity variation of a thin gold film, *Sensors And Actuators. B* 114, 513-521
- 488 Sabri, Y.M., Ippolito, S.J., O'Mullane, A.P., Tardio, J., Bansal, V., Bhargava S.K., 2011. Creating  
489 gold nanoprisms directly on quartz crystal microbalance electrodes for mercury fiber sensing.  
490 *Nanotechnology* 22 (30) 305501
- 491 Sabri, Y.M., Ippolito, S.J., Tardio, J., Atanacio, A.J., Sood, D.K., Bhargava, S.K., 2009. Mercury  
492 diffusion in gold and silver thin film electrodes on quartz crystal microbalance sensors. *Sensors and*  
493 *Actuators B* 137 246–252
- 494 Sánchez-Rodas, D., Corns, W.T., Chen, B., Stockwell, P.B., 2010. Atomic Fluorescence  
495 Spectrometry: a suitable detection technique in speciation studies for arsenic, selenium, antimony  
496 and mercury. *J. Anal. At. Spectrom.* 25 933-946
- 497 Sderström, H.S., Bergqvist, P.A., 2004. Passive air sampling using semipermeable membrane  
498 devices at different wind-speeds in situ calibrated by performance reference compounds. *Environ.*  
499 *Sci. Technol.* 38, 4828-4834.  
500
- 501 Sprovieri, F., Pirrone, N., Bencardino, M., D'Amore, F., Carbone, F., Cinnirella, S., Mannarino, V.,  
502 Landis, M., Ebinghaus, R., Weigelt, A., Brunke, E.-G., Labuschagne, C., Martin, L., Munthe, J.,  
503 Wängberg, I., Artaxo, P., Morais, F., H. J. Barbosa, J. Brito Cairns, W., Barbante, C., del Carmen  
504 Diéguez, M., Garcia, P. E., Dommergue, A., Angot, H., Magand, O., Skov, H., Horvat, M., Kotnik,  
505 J., Read, K. A., Neves, L. M., Gawlik, B. M., Sena, F., Mashyanov, N., Vladimir, Obolkin, A., Wip,  
506 D., Feng, X. B., Zhang, H., Fu, X., Ramachandran, R., Cossa, D., Knoery, J., Maruszczak, N.,  
507 Nerentorp, M., and Norstrom, C., 2016a. Atmospheric Mercury Concentrations observed at  
508 ground-based monitoring sites globally distributed in the framework of the GMOS network, *Atmos.*  
509 *Chem. Phys.*, 16, 1–21.  
510
- 511 Sprovieri, F., Pirrone, N., Bencardino, M., D'Amore, F., Angot, H., Barbante, C., Brunke, E.G.,  
512 Arcega-Cabrera, F., Cairns, W., Comero, S., Diéguez, M., Dommergue, A., Ebinghaus, R., Feng,



- 513 X.B., Fu, X., Garcia, P. E., Gawlik, B. M., Hageström, U., Hansson, K., Horvat, M., Kotnik, J.,  
514 Labuschagne, C., Magand, O., Martin, L., Mashyanov, N., Mkololo, T., Munthe, J., Obolkin, V.,  
515 Islas M.R, Sena, F., Somerset, V., Spandow, P., Vardè, M., Walters, C., Wängberg, I., Weigelt, A.,  
516 Yang, X., Zhang, H. 2016b. Five-year records of Total Mercury Deposition flux at GMOS sites in  
517 the Northern and Southern Hemispheres Atmos. Chem. Phys. Discuss., doi:10.5194/acp-2016-517  
518
- 519 Sun, Y., Xia, Y., 2003. Gold and silver nanoparticles: A class of chromophores with colors tunable  
520 in the range from 400 to 750 nm. Analyst 128, 686–691.
- 521 Y Yuan, Y., Zhao, Y., Li, H. Li, Y., Gao, X., Zheng, C., Zhang J., 2012. Electrospun metal oxide–  
522 TiO<sub>2</sub> nanofibers for elemental mercury removal from flue gas, Journal of Hazardous Materials,  
523 227–228, 427–435
- 524 Zampetti, E., Pantalei, S., Muzyczuk, A., Bearzotti, A., De Cesare, F., Spinella, C., Macagnano,  
525 A., 2013. A high sensitive NO<sub>2</sub> gas sensor based on PEDOT-PSS/TiO<sub>2</sub> nanofibers, Sensors and  
526 Actuators B 176, 390-398
- 527 Zhang, W., Tong, Y.D., Hu, D., Ou, L.B., Wang, X.J., 2012. Characterization of atmospheric  
528 mercury concentrations along an urban-rural gradient using a newly developed passive sampler.  
529 Atmos. Environ. 47, 26-32.  
530